W02

hep-ex/0106085

Experimental Status of Photon Photon into Baryon Antibaryon Pairs

T. Barillari
University of Colorado, Boulder

The exclusive production of $B\overline{B}$ pairs in the collisions of two quasi-real photons have been studied in different experiments at e^+e^- colliders. Results are presented for the processes $\gamma\gamma \to p\overline{p}$ and $\gamma\gamma \to \Lambda\overline{\Lambda}$. The cross-section measurements are compared with the recent analytic calculations based on the quark-diquark model predictions. Monte Carlo studies have been done to investigate the PEP-N expectations for the $\gamma\gamma \to p\overline{p}$ process.

1. INTRODUCTION

The exclusive production of baryon-antibaryon pairs in the collision of two quasi real photons can be used to test QCD predictions. The photons are emitted by the beam electrons and positrons and the $B\overline{B}$ are produced in the process $e^+e^- \to e^+e^-\gamma\gamma \to e^+e^-B\overline{B}$.

The application of QCD to exclusive two-photon reactions is based on the work of Brodsky and Lepage [1]. According to their formalism the process is factorized into a non-perturbative part, the hadronic wave function of the final state, and a perturbative part. A calculation based on this ansatz [2, 3] uses a specific model of the proton's three-quark wave function by Chernyak and Zhitnitsky [4]. This calculation predicts cross-sections that are about one order of magnitude smaller than the existing experimental results [5–11], for two-photon center-of-mass energies W greater than 2.5 GeV.

To model non-perturbative effects, the introduction of diquarks has been proposed [12]. Within this model, baryons are viewed as systems of quarks and diquarks, quasi-elementary constituents which partially survive medium-hard collision. Their composite nature is taken into account by diquark form factors. Recent studies [13] have extended the investigation of exclusive reactions within the diquark model to two-photon reactions [14–17].

The quark-diquark model works rather well for exclusive reactions in the space-like region [15, 18, 19]. The calculations of the integrated cross-sections for the processes $\gamma\gamma \to p\overline{p}$ and $\gamma\gamma \to \Lambda\overline{\Lambda}$ in the angular region $|\cos\theta^*| < 0.6$, θ^* here is the the polar angle of the $\gamma\gamma$ centre-of-mass system (cms), show a good agreement with the existing data described in Section 3 and Section 4 in this paper. The $\gamma\gamma \to p\overline{p}$ Monte Carlo studies for PEP-N are given in Secsection 5.

2. THEORY

2.1. Two-photon physics at e^+e^- storage rings

The two-photon process is a two step process: first both incident particles emit virtual photons with squared masses q_1^2, q_2^2 and energies w_1, w_2. Next the two photons produce the final state X. The first step, the eeγ vertex, is completely specified by quantum electrodynamics (QED); the second step, $\gamma\gamma \to X$, is not rigorously calculable for an hadronic final state X. An approximation for the cross-section can be obtained if the essential features of both eeγ vertices are given: the $1/q_i^2$-dependence from the photon propagator together with the $1/w_i$ dependence characteristic of bremsstrahlung.

A natural way of differentiating between final states X produced by the two-photon process and those produced by the e^+e^- annihilation process is the observation of a scattered electron, called "tag." Depending on the number of electrons detected (zero, one or two) events are referred to as no-tag, single-tag or double-tag, respectively. In a no-tag event the scattered electrons go undetected in the beam pipe. Consequently, the final-state X coming from the reaction $e^+e^- \to e^+e^-X$ has a small transverse momentum. If X then decays into two charged particles, usually these particles are detected at small angles with respect to the beam. They are back-to-back in the x–y plane, but in the x–z plane they are not. The $\gamma\gamma$ center of mass is moving and boosted along the beam axis. The higher the momentum, the closer are the produced particles to the beam direction. This feature, combined with the typically low mass of two-photon produced final states, severely limits the detection efficiency which rarely exceeds 10%.

2.2. Hard Scattering Picture (HSP)

In the perturbative QCD scheme, also called hard-scattering-picture (HSP) see [1, 4, 20–23], an exclusive hadronic process, $A+B \to C+D$, to leading order in the inverse of the large momentum transfer in the transverse direction, $1/p_\perp$, is described

by an exclusive hadronic amplitude $\mathcal{M}$. This amplitude can be expressed as a convolution of process-independent distribution amplitudes, ϕ_{H_i}, with the elementary scattering amplitude, T_H

$$\mathcal{M} = \int_0^1 T_H(x_j, p_\perp) \prod_{H_i} \left(\phi_{H_i}(x_j, \tilde{p}_\perp) \times \delta(1 - \sum_{k=1}^{n_i} x_k) \prod_{j=1}^{n_i} d\,x_j \right), \quad (1)$$

where $\tilde{p}_\perp \approx min(x_j, 1-x_j)\sqrt{s}|\sin\theta|$.

Eq. (1) separates the hard-scattering amplitude from the bound state dynamics, namely the short-range from the long-range phenomena.

One important phenomenological consequence coming from this factorization formula is the *dimensional counting rules*. By ignoring logarithmic corrections [24, 25], the dimensional counting rules predict the following power-law behavior of the $\gamma\gamma \to B\overline{B}$ (B = Baryons) cross-section at fixed angles:

$$\left(\frac{d\sigma_{\gamma\gamma\to B\overline{B}}}{dt}\right) \sim s^{-6}. \quad (2)$$

The scaling law is valid only at sufficiently large $p_\perp^2$ when $\alpha_s(p_\perp^2)$ is small enough to make the Feynman diagram expansion meaningful.

Another important consequence of Eq. (1) is the *hadron helicity conservation rules*. For each exclusive reaction $A+B \to C+D$, the sum of the initial helicities equals the sum of the final ones [26]:

$$\lambda_A + \lambda_B = \lambda_C + \lambda_D. \quad (3)$$

The *dimensional counting rules* are in good agreement with the data [28–30]. However, the *hadron helicity conservation* rule has given some troubles when its consequences are compared with the existing spin data in exclusive hadronic reactions. An example of a typical problem that raises from the Eq. (3), comes from the η_c and χ_0 decays into $p\overline{p}$ (see [31, 33]).

2.3. Spin problems and the diquark solution

The introduction of diquarks at this point may have two positive consequences. The first consequence is that it modifies the dimensional counting rules of Eq. (2) by effectively decreasing the number of constituents to be taken into account in the process studied. The power law behavior of the cross-section for e.g. the $\gamma\gamma \to p\overline{p}$ process [14] is then given by:

$$\left(\frac{d\sigma_{\gamma\gamma\to B\overline{B}}}{dt}\right) \sim s^{-4}. \quad (4)$$

The second consequence of diquarks as constituents has to do with the violation of Eq. (3). This violation can only come from couplings between gluons and those partons that allow helicity flips, such as vector diquarks. Again, at very large Q^2 values, if a diquark resolves into two quarks, the helicity-conservation rule is recovered, while at Q^2 values where the diquarks act as elementary objects helicity conservation can be strongly violated, which solves the quark model spin problems.

From all the applications analyzed, see summary given in [27], it emerges that diquarks seem to be a useful phenomenological way of modeling higher-order and non-perturbative effects in order to achieve a better description of many hadronic exclusive reactions. Nevertheless, the treatment of exclusive processes in the framework of constituent models and perturbative QCD is really far from being understood in a unique and well defined computational scheme.

2.4. Two-Photon annihilation into baryon-anti-baryon pairs

There are recent applications of the quark-diquark model that concern the class of reactions $\gamma\gamma \to B\overline{B}$ [13], where B represents an octet baryon (B = p, Λ, Ξ, etc.). In the older calculations of [14] the $\gamma\gamma \to p\overline{p}$ annihilation has been computed in the scheme of [1, 20]. Diquarks in this work are considered as quasi-elementary constituents, all the masses are neglected except those of the scalar diquarks in the propagator. Within the new calculations of [13], baryon-mass effects are instead taken into account, and the cross-sections have been computed down to energy values of 2.2 GeV. At these values the diquark model starts to loose its validity, but this is where most of the experiments have their bulk of data.

3. THE $\gamma\gamma \to p\overline{p}$ PROCESS

There are recent studies for the exclusive $\gamma\gamma \to p\overline{p}$ cross-section measurements using the OPAL data at LEP2, $\sqrt{s} =$ 183 and 189 GeV (see [11]). The $\gamma\gamma \to p\overline{p}$ events are selected in OPAL by applying the following main set of cuts:

1. Exactly two oppositely charged tracks; the tracks must have at least 20 hits in the central jet chamber. The selected tracks must have a minimal distance, $|d_0|$, of at most 1 cm from the beam axis.

2. For each track the polar angle must be in the range $|\cos\theta| < 0.75$ and the transverse momentum $p_\perp$ must be larger than 400 MeV. These cuts ensure a high trigger efficiency and good particle identification.

3. The polar angle in the $\gamma\gamma \to p\overline{p}$ cms has to be in the range $|\cos\theta^*| < 0.6$.

4. Data and Monte Carlo events must pass a defined trigger condition based on a combination of track and time-of-flight triggers.

5. Exclusive two-particle final states are selected by rejecting events if the transverse component of the momentum sum squared of the two tracks, $|\sum \vec{p}_\perp|^2$, is larger than $0.1\,\mathrm{GeV}^2$.

6. The large background from other exclusive processes, mainly the production of e^+e^-, $\mu^+\mu^-$, $\pi^+\pi^-$ and K^+K^- pairs, is reduced by particle identification using the specific energy loss cuts, dE/dx. The dE/dx probabilities of the tracks must be consistent with the p and $\bar{p}$ hypothesis.

Within the applied $|\cos\theta^*| < 0.6$ cut, the typical OPAL detection efficiency is about 2% at high values of W and about $7-11\%$ at low W. Similar values of detection efficiency are also found in other experiments: e.g. the TASSO [5] detection efficiency, was found to be $1.0 \pm 0.17\%$ at $W = 2.0\,\text{GeV}$, $6.5 \pm 0.6\%$ at 2.5 GeV and $3.0 \pm 0.6\%$ at 3.1 GeV.

The OPAL trigger efficiency for $p_\perp > 400\,\text{MeV}$ and for $W > 2.15\,\text{GeV}$ is about 94%. In VENUS the trigger efficiency for tracks with $p_\perp \geq 600\,\text{MeV}$ was about 97%.

3.1. Cross-section measurements

The list of the existing exclusive $\gamma\gamma \to p\bar{p}$ cross-section measurements are given in Table I. The OPAL data are not published yet, therefore they are not shown here. In Figure 1 (top) the latest VENUS [10] and CLEO [9] results are compared to the cross-section measurements obtained by TASSO [5], JADE [6], TPC/2γ [7], ARGUS [8]. Also shown in the figure are the quark-diquark model predictions [13]. A large spread of data is visible in this figure. The CLEO [9] results can be considered the most precise measurements, and they lie in the center of the other data points.

Figure 1 (bottom) shows the VENUS and CLEO cross-section measurements as function of W together with the most recent quark-diquark model predictions [13] (solid line in the figure) and the previous calculations of [12, 16] (dash-dotted line).

This figure shows that at low W the VENUS measurements are larger than the CLEO results. There is good agreement between these two measurements in the higher W region: $W > 2.6\,\text{GeV}$. The CLEO results show here a good agreement with the most recent quark-diquark model [13] in the low invariant mass region, the VENUS results lie instead above these predictions. In the higher W region the VENUS and CLEO data lie below the predictions of [13]. Within the statistical errors these measurements, in the high invariant mass region, can be considered in agreement with the calculations of [12, 16]. The preference of either quark-diquark model of [13] and of [12, 16] respectively is not obvious from the results shown in this figure.

Finally, the power law predictions of Eq. (2), for $W^2 = s$ using the fixed exponents -6, and -4 are also shown in Figure 1 (bottom). More data at both higher and lower values of W are needed to determine which is the correct power law to choose to describe the data.

Figure 2 (top) shows the VENUS and CLEO measured differential cross-sections as function of $|\cos\theta^*|$ in the range of $2.15\,\text{GeV} < W < 2.55\,\text{GeV}$. In the two experiments the differential cross-section decreases toward $|\cos\theta^*| = 0.6$. The scaled CLEO measurement lies below the VENUS results. The scaling factor used to shift the CLEO differential cross-section

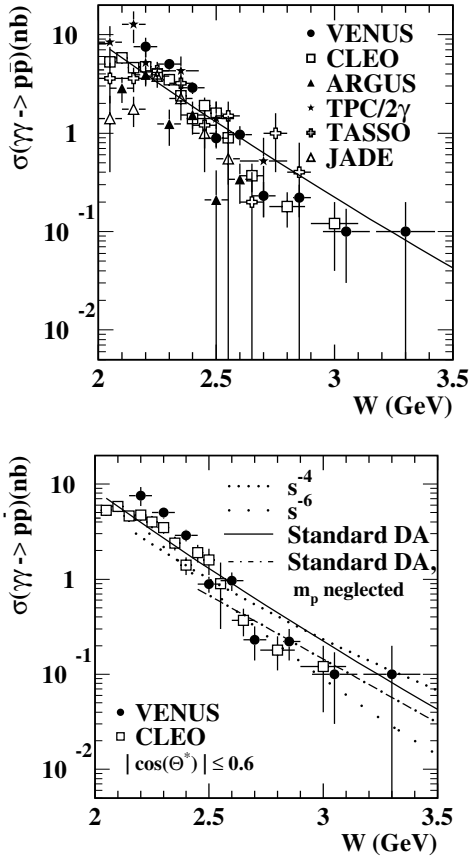

Figure 1: Cross-sections $\sigma(\gamma\gamma \to p\bar{p})$ as a function of W for $|\cos\theta^*| < 0.6$. In the figure on top the latest data obtained in VENUS [10] and CLEO [9] are compared to other experimental results [5–8]; and to the quark-diquark model predictions [13] (solid line). Here only statistical errors are shown. In the figure on the bottom the VENUS and CLEO data are shown together with the quark-diquark model of [12, 16] (dash-dotted line), and of [13] (solid line), and with the power law predictions with the fixed exponents -6, and -4. In this picture the error bars are statistical only.

measurements from the range of W between 2.0–2.5 GeV to the range of $W = 2.15$–$2.55\,\text{GeV}$ used by VENUS, is 0.6345. This scaling factor is computed by dividing the two CLEO total cross-sections integrated over the two considered W ranges of 2.0–2.5 GeV and 2.15–2.55 GeV.

Figure 2 (bottom) shows the measured differential cross-section as function of $|\cos\theta^*|$ in the high W region: $2.55\,\text{GeV} < W < 3.05\,\text{GeV}$ for VENUS and $2.5\,\text{GeV} < 3.0\,\text{GeV}$ for CLEO. There is good agreement between the results obtained by these two experiments.

Figure 3 (top) shows the comparison of the VENUS and CLEO differential cross-section measurements for the higher W region with the calculation given in [13] at $W = 2.8\,\text{GeV}$ for different distribution amplitudes (DA). The results of the pure quark model [2, 3] are also shown. The pure quark model and the quark-diquark model predictions, lie below the data but in both cases the shape is reasonably well reproduced. This could indicate that the *hadron helicity conservation rules* of

Table I The experiments that have measured the $\gamma\gamma \to p\bar{p}$ cross section in e^+e^- collision; the table gives the beam energy, the integrated luminosity, the range of W and the total number of $p\bar{p}$ events. The last line summarizes the PEP-N expectation.

e^+e^- Experiments	Year	E_{Beam} (GeV)	Integrated Luminosity (pb^{-1})	$W_{\gamma\gamma}$ (GeV)	Number of $p\bar{p}$ events
TASSO (DESY)	1982	$15 - 18.3$	19.685	$2.0 - 2.6$	8
TASSO (DESY)	1983	17	74	$2.0 - 3.1$	72
JADE (DESY)	1986	$17.4 - 21.9$	$59.3 + 24.2$	$2.0 - 2.6$	41
TPC/2γ (SLAC)	1987	14.5	75	$2.0 - 2.8$	50
ARGUS (DESY)	1989	$4.5 - 5.3$	234	$2.6 - 3.0$	60
CLEO (CESR)	1994	5.29	1310	$2.0 - 3.25$	484
VENUS (TRISTAN)	1997	$57 - 64$	331	$2.2 - 3.3$	311
PEP-N (SLAC)	-	$0.5_{(VLER)} - 3.1_{(LER)}$	200	$1.9 - 2.6$	60

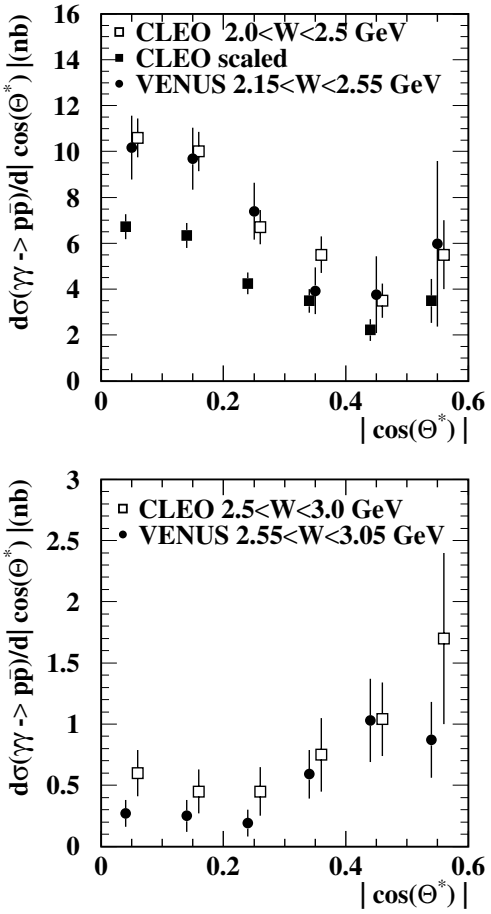

Figure 2: Differential cross-sections for $\gamma\gamma \to p\bar{p}$ as a function of $|\cos\theta^*|$. Data from [9, 10] are for a low range of W, $2.15\,\text{GeV} < W < 2.55\,\text{GeV}$ (top), and the high range of W (bottom), $2.5\,\text{GeV} < W < 3.0\,\text{GeV}$ for CLEO and $2.55\,\text{GeV} < W < 3.05\,\text{GeV}$ for VENUS. Errors are statistical only.

Eq. (3) are satisfied in the high W region but they are not in the low W values. In fact, in this low W region the measured differential cross-sections have a different distribution from the differential cross-sections obtained in the high invariant mass region.

The different shape of the curves in these figures shows also that for low W the perturbative calculations of [2, 3] are not valid and the $p\bar{p}$ system might be described as a bound system with orbital angular momentum greater than zero.

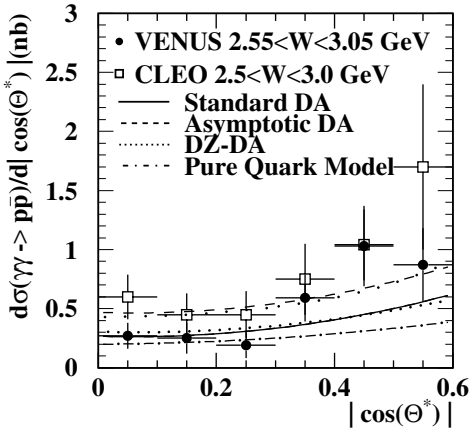

Figure 3: VENUS and CLEO differential cross-section $d\sigma(\gamma\gamma \to p\bar{p})/d|\cos\theta^*|$, shown with statistical and systematic errors, in the range $2.55\,\text{GeV} < W < 3.05\,\text{GeV}$ for VENUS and $2.5\,\text{GeV} < W < 3.0\,\text{GeV}$ for CLEO compared to the theoretical predictions given in [2] (dash-dotted line), in [12, 16] (dotted line), and in [13] (the other lines) for $|\cos\theta^*| < 0.6$.

4. THE $\gamma\gamma \to \Lambda\overline{\Lambda}$ PROCESS

The exclusive cross-section measurement for the $\gamma\gamma \to \Lambda\overline{\Lambda}$ process and the inclusive reaction $e^+e^- \to e^+e^-\Lambda\overline{\Lambda}X$ have been studied by CLEO [37] and by L3 [38], respectively. The results of the integrated $\gamma\gamma \to \Lambda\overline{\Lambda}$ cross-section ($|\cos\theta^*| < 0.6$) obtained by CLEO [37] (Figure 4) show a better agreement with the most recent quark-diquark predictions [13] than compared with the old results of [15]. In the low invariant masses region the data shows a discrepancy with the model. This discrepancy can be explained by the lower limit of applicability of the quark-diquark model itself [13]. In Figure 5 (top) the L3 cross-section measurements [38] $\sigma(\gamma\gamma \to \Lambda\overline{\Lambda}X)$

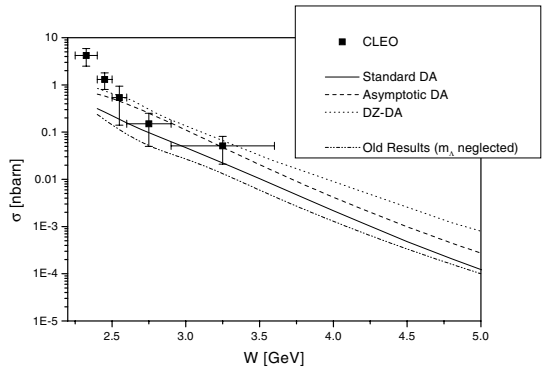

Figure 4: CLEO [37] integrated cross-section for $\gamma\gamma \to \Lambda\overline{\Lambda}$ measurement compared with the theoretical results of [13, 15]

are shown together with the CLEO results. The two measurements can be considered in agreement within large errors. The comparison of the L3 [38] data with the most recent quark-diquark model predictions [13] for the three different distribution amplitudes is shown in Figure 5 (bottom). The L3 measurements lie above but still in agreement with the predictions. The excess shown in the data may be due to the $\Sigma^0\overline{\Sigma^0}$ and other baryons contamination not removed from the sample of events analyzed.

5. PEP-N EXPECTATIONS

To understand the possibility of selecting two-photon events and in particular $\gamma\gamma \to p\overline{p}$ events at PEP-N, preliminary Monte Carlo distributions have been studied. Some quantities are plotted in Figure 6. The $\gamma\gamma \to p\overline{p}$ Monte Carlo events have been simulated with the GALUGA [35, 36] generator within a range of W between 2 and 2.5 GeV. Due to the beam asymmetry the $\gamma\gamma$ cms receives a larger boost compared to a symmetric e^+e^- machine and therefore the momenta of the final state particles are larger. Figure 6 (top) shows that the proton momentum distribution varies between $0.6 - 2.0$ GeV instead e.g. of the range 0.4–1.1 GeV observed for the proton momenta in OPAL [11]. Figure 6 (bottom) shows the $|\cos\theta_{\rm LAB}|$[1] distribution. These two distributions show the better experimental conditions expected at PEP-N for two-photon events. A high detection efficiency, large angular acceptance, and a good trigger efficiency due to the higher momentum tracks are anticipated. The last row in Table I gives the number of $\gamma\gamma \to p\overline{p}$ events expected to be detected at PEP-N under the assumption of a good trigger and detection efficiency and for a total integrated luminosity of 200 pb^{-1}.

[1] $\theta_{\rm LAB}$ is the polar angle in the laboratory

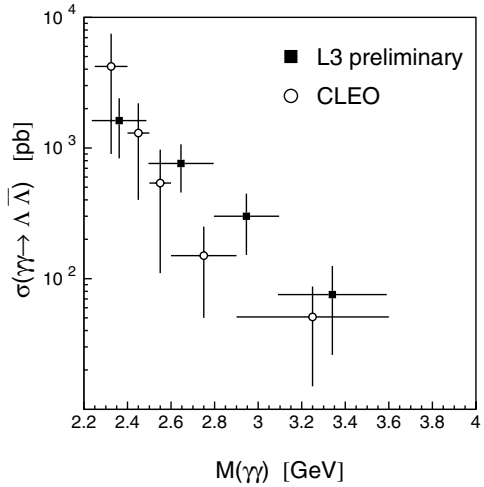

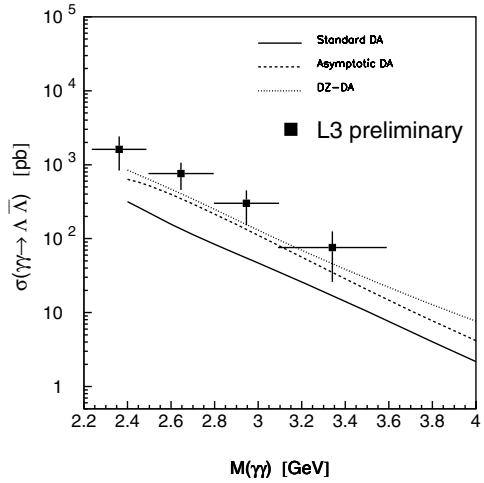

Figure 5: The L3 [38] integrated cross-section $\sigma(\gamma\gamma \to \Lambda\overline{\Lambda}X)$ is compared with the CLEO $\sigma(\gamma\gamma \to \Lambda\overline{\Lambda}$ measurements (top) and the quark-diquark model predictions of [13] (bottom).

6. CONCLUSION

The data shown in this paper indicate that there is still a lot to investigate about the exclusive $\gamma\gamma \to B\overline{B}$ processes. The expected good experimental conditions at PEP-N would make it the ideal place to continue these studies, especially in the low invariant mass region.

7. ACKNOWLEDGMENT

I would like to thank R. Baldini and S.J. Brodsky for gently inviting me to present this work at the PEP-N workshop.

REFERENCES

[1] S. J. Brodsky and G. P. Lepage , Phys. Rev. **D22** (1980) 2157.

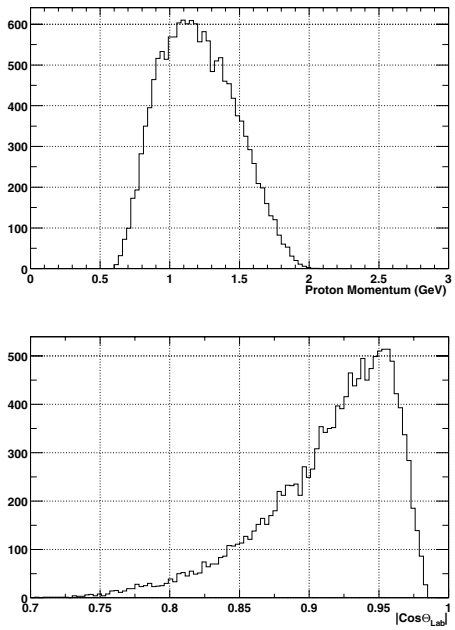

Figure 6: Monte Carlo events distributions for PEP-N at $\sqrt{s} = 2.5\,\mathrm{GeV}$ and for beam energies of $3.1\,\mathrm{GeV}_{\mathrm{LER}}$, $0.5\,\mathrm{GeV}_{VLER}$: (top) proton momentum distribution; bottom $|\cos\theta_{\mathrm{LAB}}|$ distribution.

[2] G. R. Farrar, E. Maina, and F. Neri, Nucl. Phys. **B259** (1985) 702.

[3] J. F. Gunion and D. Millers, Phys. Rev. **D34** (1986) 2657.

[4] V. L. Chernyak and I. R. Zhitnitsky, Nucl. Phys. **B246** (1984) 52.

[5] TASSO, M. Althoff et al., Phys. Lett. **B130** (1983) 449.

[6] JADE, W. Bartel et al., Phys. Lett. **B174** (1986) 350.

[7] TPC/Two Gamma, H. Aihara et al., Phys. Rev. **D36** (1987) 3506.

[8] ARGUS, H. Albrecht et al., Z. Phys. **C42** (1989) 543.

[9] CLEO, M. Artuso et al., Phys. Rev. **D50** (1994) 5484.

[10] VENUS, H. Hamasaki et al., Phys. Lett. **B407** (1997) 185.

[11] T. Barillari, Cross-Section Measurements of the Process $\gamma\gamma \to \mathrm{p\overline{p}}$ in Untagged Events at $\sqrt{s} = 183$ and 189 GeV with the OPAL Detector at LEP, PhD thesis N° 3256, University of Geneva (2001).

[12] M. Anselmino, P. Kroll, and B. Pire, Z. Phys. **C36** (1987) 89.

[13] C. F. Berger, Exclusive two-photon reactions in the few GeV region, Diploma thesis, Technological University Graz (1997).

[14] M. Anselmino, F. Caruso, P. Kroll, and W. Schweiger, Int. J. Mod. Phys. **A4** (1989) 5213.

[15] P. Kroll, M. Schurmann, and W. Schweiger, Int. J. Mod. Phys. **A6** (1991a) 4107.

[16] P. Kroll, Th. Pilsner, M. Schürmann, W. Schweiger, Phys. Lett. **B316** (1993) 546

[17] P. Kroll, M. Schürmann, and P. A. M. Guichon, Nucl. Phys. **A598** (1996) 435.

[18] P. Kroll, M. Schurmann, and W. Schweiger, Z. Phys. **A342** (1992) 429.

[19] P. Kroll, M. Schurmann, and W. Schweiger, Z. Phys. **A338** (1991) 339.

[20] S. J. Brodsky and G. R. Farrar, Phys. Rev. **D11** (1975) 1309.

[21] S. J. Brodsky and G. P. Lepage, Phys. Rev. **D24** (1981) 1808.

[22] A. H. Mueller, Phys. Rept. **73** (1981) 237.

[23] J. Botts and G. Sterman, Nucl. Phys. **B325** (1989) 62.

[24] S. J. Brodsky and G. R. Farrar, Phys. Rev. Lett. **31** '(1973) 1153.

[25] V. A. Matveev, R. M. Muradian, and A. N. Tavkhelidze, Nuovo Cim. Lett. **7** (1973) 719.

[26] S. J. Brodsky and G. P. Lepage, Phys. Rev. **D24** (1981) 2848.

[27] M. Anselmino et al., Rev. Mod. Phys. **65 No. 4** (1993)

[28] R. L. Anderson et al., Phys. Rev. Lett. **30** (1973) 627.

[29] J. L. Stone and J. P. Chanowski and H. R. Gustafson and M. J. Longo and S. W. Gray Nucl. Phys. **B143** (1978) 1.

[30] R. G. Arnold et al., Phys. Rev. Lett. **57** (1986) 174.

[31] C. Baglin et al., Phys. Lett. **B172** (1986) 455.

[32] S. J. Brodsky and F. C. Erne and P. H. Damgaard and P. M. Zerwas Conribution to ECFA Workshop LEP200, Aachen, Germany Sep 29 - Oct 1, (1986).

[33] R. M. Baltrusaitis et al., Phys. Rev. **D33** (1986) 629.

[34] V. M. Budnev, I. F. Ginzburg, G. V. Meledin, and V. G. Serbo, Phys. Rep. **15** (1974) 181.

[35] G. A. Schuler, hep-ph/9611249 (1996).

[36] G. A. Schuler, Comput. Phys. Commun. **108** (1998) 279.

[37] CLEO, S. Anderson et al., Phys. Rev. **D56** (1997) 2485.

[38] L3, M. Acciarri et al., L3 Note **2566** (2000)